MIT Libraries | DSpace@MIT

MIT Open Access Articles

Aggregation and Fibril Structure of A#M01–42 and A#1–42

Massachusetts Institute of Technology

Aggregation and Fibril Structure of Aβ$_{M01-42}$ and Aβ$_{1-42}$

Robert Silvers[1], Michael T. Colvin[1,#], Kendra K. Fredrick[3,¶], Angela C. Jacavone[1,§],

Susan L. Lindquist[3,†], Sara Linse[2*], and Robert G. Griffin[1*]

Email rgg@mit.edu

[1]Department of Chemistry and Francis Bitter Magnet Laboratory

Massachusetts Institute of Technology

Cambridge, Massachusetts 02139

[2]Department of Biochemistry and Structural Biology

Lund University

SE22100 Lund, Sweden

[3]Whitehead Institute for Biomedical Research

Nine Cambridge Center

Cambridge, Massachusetts 02142

¶ Present address: Dept. of Biophysics, The University of Texas Southwestern Medical Center, 5323 Harry Hines Boulevard, Dallas, Texas, 75390

§ Present address: University of New England, 11 Hills Beach Rd, Biddeford, ME 04005

Present address: Ortho Clinical Diagnostics, 130 Indigo Creek Drive, Rochester, NY 14626

† Deceased October 27, 2016

ABSTRACT

A mechanistic understanding of Aβ aggregation and high-resolution structures of Aβ fibrils and oligomers are vital to elucidating relevant details of neurodegeneration in Alzheimer's disease, which will facilitate the rational design of diagnostic and therapeutic protocols. The most detailed and reproducible insights into structure and kinetics have been achieved using Aβ peptides produced by recombinant expression, which results in an additional methionine at the N-terminus. While the length of the C-terminus is well established to have a profound impact on the peptide's aggregation propensity, structure, and neurotoxicity, the impact of the N-terminal methionine on the aggregation pathways and structure is unclear. For this reason, we have developed a protocol to produce recombinant Aβ$_{1-42}$, *sans* the N-terminal methionine, using an N-terminal SUMO-Aβ$_{1-42}$ fusion protein in reasonable yield, with which we compared aggregation kinetics with Aβ$_{M01-42}$ containing the additional methionine residue. The data revealed that Aβ$_{1-42}$ and Aβ$_{M01-42}$ aggregate with similar rates and by the same mechanism, in which the generation of new aggregates is dominated by secondary nucleation of monomers on fibrils surface. We also recorded MAS NMR spectra that demonstrated that excellent spectral resolution is maintained with both Aβ$_{M01-42}$ and Aβ$_{1-42}$ and that the chemical shifts are virtually identical in dipolar recoupling experiments that provide information about rigid residues. Collectively, these results indicate that the structure of the fibril core is unaffected by N-terminal methionine. This is consistent with the recent structures of Aβ$_{M01-42}$ where the M$_0$ is located at the terminus of a disordered 14 amino acid N-terminal tail.

INTRODUCTION

Amyloid fibril formation is associated with over 40 diseases[1] including Alzheimer's disease,[2] Parkinson's disease,[3-6] type II diabetes[7, 8], and dialysis-related amyloidosis.[9, 10] Of these, Alzheimer's disease (AD) is the most prevalent, currently affecting an estimated 5.5 million Americans according to the Alzheimer's Association. By 2050 the patient population is expected to grow to 16 million people, providing an imperative to develop diagnostic and therapeutic protocols to address AD. Multiple lines of evidence indicate that the aggregation of β-amyloid (Aβ) peptide is integral to the disease pathogenicity. Aβ peptides are generated by the cleavage of the amyloid precursor protein (APP) by the membrane associated β- and γ-secretases,[11, 12] yielding a variety of Aβ with different lengths, the two most common being $A\beta_{1-40}$ (APP 672-711) and $A\beta_{1-42}$ (APP 672-713). The former is more abundant and the latter is significantly more amyloidogenic and neurotoxic.[13, 14] The difference between the two isoforms is the addition of I41 and A42 (APP 712-713), which dramatically alters the aggregation kinetics,[15] neurotoxicity,[16] and structure.[17-19] Furthermore, it has recently been demonstrated that $A\beta_{M01-40}$ and $A\beta_{M01-42}$ do not cross seed one another, while each one is highly efficient in self-seeding, suggesting as well that fibrils of $A\beta_{40}$ and $A\beta_{42}$ possess different structures.[17, 20]

A more detailed understanding of Aβ in its various aggregated forms is vital to determining its pathogenicity and structure, both of which are necessary for rational design and development of diagnostic and therapeutic tools. To that end, substantial efforts have been devoted to understanding the details associated with the mechanism of aggregation as well as aggregate structure and how these features relate to toxicity [1, 21-23]. Aβ fibrils are sparingly soluble and do not diffract to high resolution, rendering conventional tools for biological structure determination such as solution NMR spectroscopy and X-ray diffraction of limited utility in characterizing fibril samples. Fortunately, magic angle spinning (MAS) nuclear magnetic resonance (NMR) spectroscopy has proven to be a powerful

technique to elucidate the structural details of amyloid fibrils on an atomic level, including backbone conformations, supramolecular organization, and registry of inter-strand arrangements of amyloid fibrils.[24-26]

Because of their relatively short length, $A\beta_{1-40}$ and $A\beta_{1-42}$ peptides used in MAS NMR spectroscopy and in many other biophysical studies have historically been prepared via peptide synthesis. In the case of NMR experiments, this permits specific labeling of individual residues that was necessary because of the broad linewidths (2-4 ppm) observed in early spectra.[27-29] However, the recent report that recombinant $A\beta_{1-42}$ aggregates significantly faster and is more neurotoxic when compared with synthetic $A\beta_{1-42}$[16] has stimulated significant interest in developing recombinant methods for preparation. In particular, recombinant $A\beta$ is more neurotoxic in cultured rat primary cortical neurons, and more toxic *in vivo*, as demonstrated by enhanced induction of abnormal phosphorylation of tau leading to tau aggregation into neurofibrillary tangles in brains of transgenic mice. [16] Recombinant $A\beta_{1-42}$ is therefore likely more relevant to the pathogenicity of AD than is synthetic protein.[16] The origin of the differences between synthetic and recombinant $A\beta$ are not completely understood, but could be due to racemization and/or coupling errors that occur during synthesis leading to a large number of similar sequences. Such impurities are very difficult to separate. In contrast, recombinant expression in for example *E. coli* provides excellent fidelity with respect to both sequence homogeneity and chirality. Finally, for NMR structure experiments it is desirable to prepare uniformly $^{13}C,^{15}N$ labeled $A\beta$ samples and the most cost effective approach to producing such samples is biosynthesis (*vide infra*). Thus, it is critical to have a robust biosynthetic method of preparation of $A\beta$ for the many biophysical and structural studies of this important peptide.

Over the past decade, MAS NMR has become the method of choice to characterize amyloids including PI3-SH3,[30, 31] β_2-microglobulin,[9, 32-34] α-synuclein[3, 35-47] and $A\beta$.[17, 19, 20, 48-52] To obtain an

atomic level structure, it is necessary to complete spectral assignments of all residues and assemble an extensive set of distance constraints (>5 per residue). This typically requires a set of chemically identical peptides with different isotopic labeling to generate 2D and 3D correlation spectra combined with a series of dipolar recoupling experiments to generate inter- and intra-molecular constraints. Uniform $^{13}C/^{15}N$ labeling of proteins is easily performed when expressed recombinantly, and partial labeling is achieved with schemes utilizing $^{15}NH_4Cl$ as the source of ^{15}N and 1,6-$^{13}C_2$-glucose, 1,3-$^{13}C_2$-glycerol, 2-$^{13}C_1$-glycerol, or REDOX labeling using ^{13}C acetate[53] as the ^{13}C source. All of these approaches are feasible and have been found to yield inter- and intra-molecular constraints, and minimize dipolar truncation allowing for long distance correlation experiments.

Currently several methods exist to produce recombinant Aβ containing an N-terminal methionine. Its small size and its propensity to aggregate permit direct expression resulting in the formation of inclusion bodies. This approach has been widely used to prepare Aβ due to the ease of production and purification.[54] Although this method is effective, it leaves an N-terminal methionine (M_0) residue whose impact on the aggregation of Aβ and the fibril structure is as yet unknown. Peptides cleaved just before M671 have to our knowledge not been observed in human samples, even though in APP, M671 precedes D672, numbered D1 in the released Aβ peptides, many variants with extended N-termini are found in blood and CSF [55, 56] Furthermore, while N-terminal extension of $Aβ_{42}$ with 5-40 residues from APP has been found to retard aggregation in a manner proportional to the length of the extension[57] the effect of the N-terminal methionine in $Aβ_{M01-42}$ on the aggregation mechanism and rate remains to be found.

$Aβ_{M01-40}$, $Aβ_{M01-42}$, as well as the N-terminally extended variants all aggregate by the same general mechanism, which relies on at least three microscopic steps: primary nucleation of monomers in solution, elongation by monomer addition at fibril ends and secondary nucleation of monomers on fibril surfaces.[15, 57, 58] The difference between the Aβ length variants lies in the rate constants of these three

processes and one could imagine that the N-terminal methionine may have an impact on some rate constants or produce structurally different Aβ fibrils from those produced *sans* the N-terminal methionine. One can avoid the presence of the N-terminal methionine by utilizing an N-terminal fusion protein, and several methods have been reported which utilize various fusion proteins in recombinant expression of Aβ.[59] These include glutathione-S-transferase,[60] ubiquitin,[61] intestinal fatty acid binding protein (IFABP)[62], hen-egg lysozyme[63] and NANP.[64] Although these preparations were used previously, they were typically for Aβ$_{1-40}$ and the yields reported make it challenging to generate sufficient material to fill an MAS NMR rotor (~30 mgs). Recently a preparation using SUMO (small ubiquitin-like modifier) as an N-terminal fusion protein was reported, which possessed excellent protein overexpression yields in rich media.[65, 66]

Here, we chose to utilize this construct to overexpress the SUMO-Aβ$_{1-42}$ fusion protein in isotopically enriched minimal media and have modified the purification to produce sufficient quantities of Aβ monomers for kinetic experiments and subsequently for fibrils for MAS NMR spectra. Measurements of the aggregation kinetics revealed only very small differences between Aβ$_{M01-42}$ and Aβ$_{1-42}$, all rate constants are within a factor of 2.5, and this along with the ability of Aβ$_{M01-42}$ and Aβ$_{1-42}$ to cross seed each other, suggest that both the mechanism of aggregation and fibril structure are highly similar. For more detailed structural comparison, we compared the MAS NMR spectra of Aβ$_{M01-42}$ with Aβ$_{1-42}$ and found few chemical shift differences among residues in the fibril core. Thus, the presence of an additional methionine on the N-terminus has little impact on the aggregation rate, or fibril core structure as ascertained by MAS NMR. More explicitly, these findings indicate that the mechanism of aggregation is likely similar, and that the microscopic structure of the amyloid core is identical.

EXPERIMENTAL

Preparation of SUMO-Hydroxlyase. The expression and purification of His$_6$-tagged SUMO-1 protease (ULP-1-His$_6$) has been described in detail previously,[67] and is summarized below. The plasmid coding for ULP-1-His$_6$ was kindly provided by Dr. Jens Tyedmers (University Heidelberg, Germany). ULP-1-His$_6$ was overexpressed in *E. coli* BL21 (DE3) by inoculating 100 mL of LB medium by a single colony and was grown overnight at 30°C. 5 mL of the overnight culture was added to 1 L of LB broth and grown at 30°C until an OD$_{600}$=1.0 was reached. Subsequently the temperature was lowered to 20°C followed by addition of 0.5 mM isopropyl β-D-1-thiogalactopyranoside (IPTG) one hour after temperature change. Expression were conducted over night and cells were subsequently harvested and stored at -80°C. The pellet was subjected to two freeze-thaw cycles (frozen in liquid N$_2$ and thawed in a 45°C water bath) and resuspended in a buffer containing 40 mM HEPES/KOH pH 7.4, 150 mM KCl and 20 mM β-mercaptoethanol (buffer A), followed by addition of 10 mg lysozyme, 0.5 mg of DNAse, and an EDTA-free Complete® tablet. The pellet was sonicated with a tip sonicator (Branson 450 sonifier) 50 % duty cycle, 2 min followed by 2 min rest (2x) and pelleted by centrifugation for 20 min at 20.000g. The supernatant was added to 5 mL of Ni-NTA resin (GE Healthcare) and subsequently washed with 150 ml buffer A and eluted with buffer B (buffer A + 250 mM imadizole). Fractions containing protein were pooled. The eluted protein was placed into 10 kDa snakeskin dialysis tube and left to dialyze for 2 days at 4°C in 40 mM HEPES/KOH pH 7.4, 100 mM KCl, and 10 mM β-mercaptoethanol with 3 buffer changes every 12 h, 4 L each. Following dialysis, the sample was concentrated using a 10 kDa centrifugal concentrator to a final volume of 2 mL with an equal volume of glycerol added, and 100 µL aliquots were stored at -80°C until used.

Preparation of Aβ$_{1-42}$. DNA coding for SUMO and Aβ was extracted from commercial vectors and prepared by *de novo* gene synthesis, respectively, and overlapped via PCR to generate a chimeric

construct of SUMO fused with $A\beta_{1-42}$ containing the gateway handles (e.g. attR1 and attR2). The DNA coding for SUMO-$A\beta_{1-42}$ was inserted into a pDEST17 vector containing an N-terminal His$_6$ tag via gateway cloning and transformed into BL21 Star (DE3) pLysS cells (Invitrogen), individual colonies were sent for DNA sequencing, and appropriate colonies were cultured overnight in 5 mL of LB broth (100 μg/mL ampicillin and 38 μg/mL of chloramphenicol), with glycerol stocks prepared the following morning. 200 μL of the glycerol stock was plated onto LB agar containing 100 μg/mL ampicillin and 38 μg/mL of chloramphenicol and grown overnight at 37°C. Several single colonies were used to inoculate 50 mL LB medium containing 100 μg/mL ampicillin and 38 μg/mL of chloramphenicol and cultured over night at 37°C. Subsequently, 1 ml of each over-night culture was used to inoculate 500 mL of M9 medium consisting of 2 g/L glucose, 1 g/L NH$_4$Cl, 2 mM MgSO$_4$, 100 μM CaCl$_2$, 10 mg/L thiamine, 10 mg/L of FeSO$_4$, 100 μg/mL ampicillin, and 38 μg/mL of chloramphenicol. Cells were grown at 37°C until an OD$_{600}$ of 0.8 was reached, at which time overexpression was induced with IPTG. Cells were allowed to express at 37°C for four hours, and were subsequently harvested by centrifugation and stored at -80°C. Typically, a final OD$_{600}$ of 1.8-2.0 was reached prior to pelleting.

Cell pellets were thawed and resuspended in 10 mM Tris pH 8.0, 1 mM EDTA (buffer C) and sonicated (Branson Sonifier 450) on ice for 2 minutes and pelleted for 10 minutes at 15,000g. The supernatant was removed, the pellet was resuspended in buffer C and sonicated three additional times, for times of 30 seconds, 20 seconds and 15 seconds, respectively, each sonication was followed by centrifugation for five minutes. Subsequently the remaining pellet was dissolved in lysis buffer (buffer C + 8 M urea) and sonicated for 2 minutes followed by 2 minutes rest (3x), followed by centrifugation at 15,000g for 15 minutes. The supernatant was decanted and subsequently diluted with buffer C by a factor of 4 to yield 2 M urea and added to 30 mL of DEAE cellulose. The protein was allowed to bind for 30-60 min, and the resin was subsequently loaded into a column. The column was then washed with

50 mL of buffer C + 2 M urea with increasing amounts of NaCl: 10 mM (2x), 25 mM (2x), 75 mM (1x), 200 mM (4x), and 500 mM (1x). We found that SUMO-Aβ_{1-42} elutes at 200 mM NaCl. The eluate was concentrated by a factor of four in a centrifugal concentrator (3.5 kDa cutoff), followed by dilution by a factor of four with buffer C, to yield 0.5 M urea in buffer C. A representative yield of the SUMO-Aβ fusion protein is ~100 mg/L M9 minimal medium. ULP-1 was added immediately after dilution and the fusion protein allowed to cleave for at least two hours at room temperature, followed by lyophylization. The lyophilized material was dissolved in 6 M GuHCl and subjected to size exclusion chormatography (GE Superdex 26/600 75pg) and eluted with buffer containing 20 mM sodium phosphate pH 8.0, 0.2 mM EDTA to isolate monomeric Aβ_{1-42}. The monomer solution contained residual SUMO domain and was therefore lyophylized, dissolved in 6 M GuHCl and subjected to size exclusion chromatography one more time. Fibrils were formed by seeding with Aβ_{M01-42}.

Aggregation kinetics by thioflavin T fluorescence. The monomer from above was lyophilized, dissolved in 6 M GuHCl and subjected to a third round of size exclusion chormatography on a gel filtration column (GE Superdex 10/300 75pg) in 2 buffer containing 20 mM sodium phosphate pH 8.0, 0.2 mM EDTA to isolate pure monomer. The monomer was diluted with the same buffer to prepare a series of samples with peptide concentration ranging from 1 to 6 µM. All samples contained 10 µM thioflavin T. The experiment was initiated by placing the 96-well plate at 37$^{\text{o}}$C in a plate reader (Fluostar Omega, Optima or Galaxy from BMG Labtech, Offenburg, Germany). The ThT fluorescence was measured through the bottom of the plate every 60 or 120 seconds (with excitation filter 440 nm, and emission filter 480 nm). The data were analyzed globally using the AmyloFit interface.[68] with the equations described in references 58 and 68

MAS NMR spectroscopy. Fully formed (mature) fibrils were packed into a 3.2 mm Bruker rotor using a home-built centrifugal packing tool. Spectra were recorded on a Bruker 800 MHz AVANCE III spectrometer equipped with a 3.2 mm triple channel HCN Bruker probe (Bruker Biospin, Billerica, MA). Spectra were recorded at $\omega_r/2\pi = 20$ kHz and regulated to ± 10 Hz using a Bruker spinning frequency controller. All experiments were conducted at 277 K. Spectra were processed using TopSpin 3.1, and analyzed in Sparky.[69]

RESULTS AND DISCUSSION

Preparation of Aβ$_{1-42}$. The SUMO fusion protein was placed N-terminally of Aβ$_{1-42}$ to eliminate the M$_0$ residue present when directly expressed in *E. coli*. Most of the SUMO-Aβ fusion protein is in the supernatant following lysis, and that it can be effectively separated using DEAE cellulose resin (data not shown). The SUMO fusion protein is cleaved by SUMO-1 protease (ULP-1-His$_6$, **Figure 1**) which recognizes and cleaves SUMO based on SUMO's tertiary structure,[67] necessitating that SUMO be refolded following lysis. We found that SUMO-Aβ has a propensity to aggregate in the absence of a denaturant and therefore the SUMO-Aβ fusion protein was cleaved with 0.5 M urea present, the highest concentration of urea that would permit reasonable cleavage yields (data not shown).

Following cleavage, Aβ$_{1-42}$ was separated from SUMO using size exclusion chromatography in an identical manner to the purification employed before preparing Aβ$_{M01-42}$ fibrils.[17, 54] The yield of Aβ$_{1-42}$ in M9 minimal medium was comparable with other protocols found in the literature and was about 20 mg/liter prior to gel filtration, which was sufficient to produce enough amyloid fibrils for characterization by MAS NMR spectroscopy. With further optimization of the purification we anticipate an increase in the yield of fusion protein and are currently exploring additional purification options to enhance the yield of Aβ.
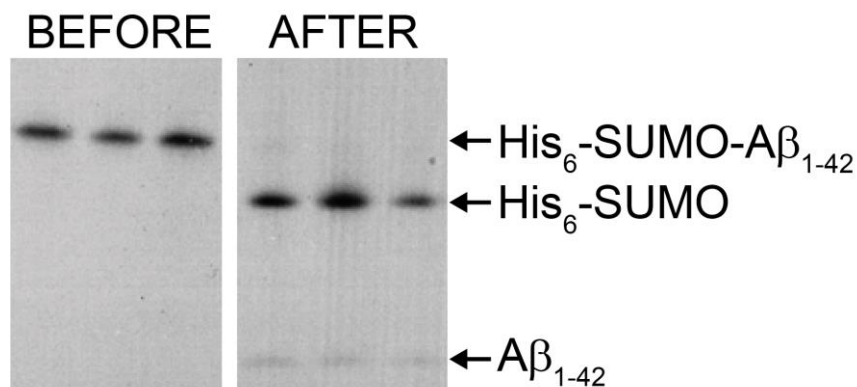

Figure 1. SDS-PAGE gel showing the cleavage with ULP-1-His$_6$. The cleavage is complete within 24 hours with 0.5 M urea present. The gel was stained using Coomassie Brilliant Blue. The three lanes in each case are repetitions of the same sample.

Aggregation kinetics of Aβ₁₋₄₂. Measuring the aggregation kinetics, which are typically monitored by thioflavin T fluorescence, followed by global fitting of the data[68] can elucidate the mechanistic details of aggregation. Recently, the aggregation of $A\beta_{M01-42}$ was shown to proceed through a secondary nucleation step, suggesting a positive feedback loop between monomers and already formed fibrils.[58] Here we examined the kinetics and concentration dependence of $A\beta_{1-42}$ aggregation to evaluate mechanistic similarities or differences between $A\beta_{M01-42}$ and $A\beta_{1-42}$. Examples of aggregation kinetics data for $A\beta_{1-42}$ are shown in **Figure 2**. The experiment was repeated three times with similar results. In comparison with previous data for $A\beta_{M01-42}$, we find that the removal of M_0 retains the shape of individual aggregation traces (**Figure 2A**) and produces a highly similar concentration dependence of the half time for fibril formation (**Figure 2B**), implying that fibrillization of both species ($A\beta_{M01-42}/A\beta_{1-42}$) occurs by a similar mechanism.[70] Fitting of a power function to the concentration dependence of the half time yields an exponent of -1.3, in agreement with earlier findings in reference 58. The AmyloFit interface[68] was used to fit various kinetic models in the form of master equations to the ThT
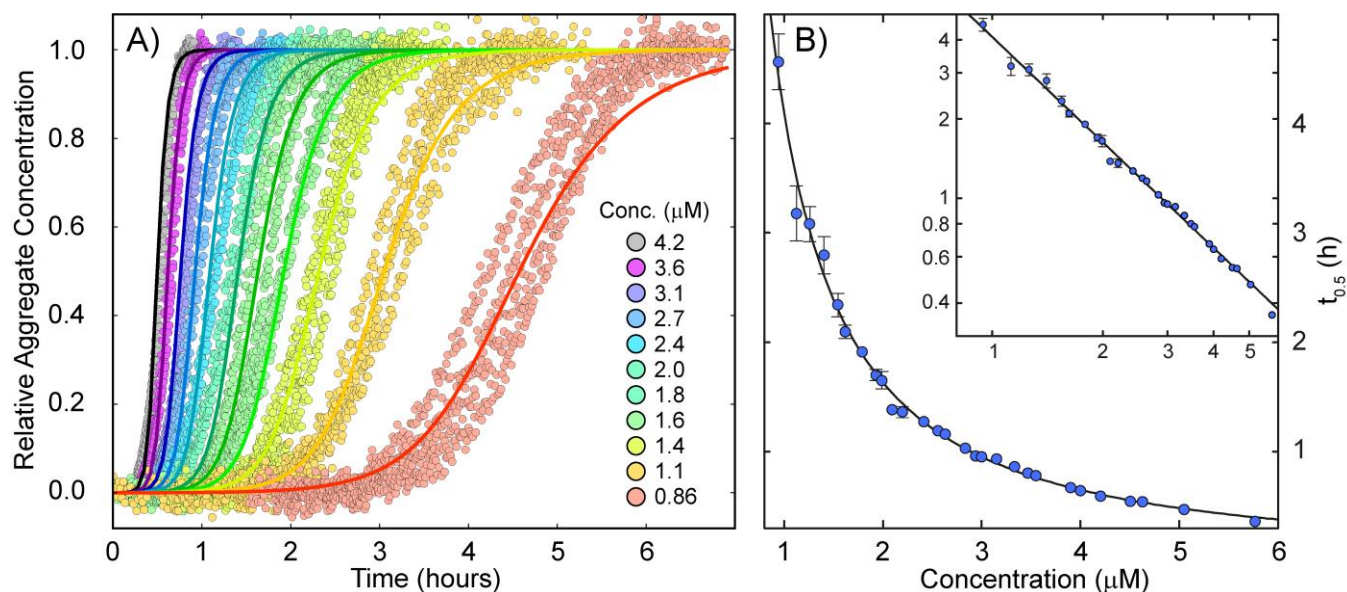

Figure 2. Kinetics monitored by thioflavin T at 37°C. A. Examples of aggregation data at 11 peptide concentrations in quadruplicate together with a global fit $k_+k_n = 900$ M^{-2}s^{-2}; $k_+k_2 = 1 \cdot 10^{11}$ M^{-3}s^{-2}). B. Half time of aggregation versus peptide concentration combined from three experiments of the type shown in panel A, plus a fitted power function with exponent -1.3.

fluorescence data for fibril formation versus time for all peptide concentrations globally. While models including only primary nucleation and elongation, or primary nucleation, elongation and fragmentation failed to fit the data, as previously found for Aβ$_{M01-42}$,[58] a model including primary nucleation, elongation and secondary nucleation produced acceptable global fits to the data as shown in Figure 2A. This analysis further revealed that all rate constants are within a factor of 2.5 when the two peptides are compared, and there is a slightly higher dominance of the secondary pathway in the shorter peptide. Still the difference between the two peptides is so small that the main finding is that there is no major change in mechanism or rate constants. For the product rate constant k_+k_2, we obtain a value of 1×10^{11} $M^{-3}s^{-2}$ for Aβ$_{1-42}$ (vs. 4×10^{10} $M^{-3}s^{-2}$ for Aβ$_{M01-42}$)[58] while we obtain similar values for the combined rate constant k_+k_n for both peptides (900 $M^{-2}s^{-2}$). As a comparison, removing two residues at the C-terminus leads to a 1800-fold reduction in k_+k_n $_{and}$ a 44-fold reduction in k_+k_2.[15] However, the minor difference in aggregation kinetics between Aβ$_{1-42}$ and Aβ$_{M01-42}$ does not provide information about the atomic level structure of the two fibrils.

Fibrils of Aβ$_{1-42}$ and Aβ$_{M01-42}$ have rigid and dynamic regions. To compare the structures of Aβ$_{M01-42}$ and Aβ$_{1-42}$, we therefore recorded MAS NMR spectra to determine what impact, if any, the N-terminal methionine has on the microscopic structure of Aβ$_{42}$ fibrils. Amyloid fibrils of Aβ$_{M01-42}$ have a rigid amyloid core that sequesters residues Q15-A42 into parallel in register beta sheets while residues M0-H14 are less ordered.[17] Overall, removal of the M0 did not result in striking change in the rigid regions of these fibrils.

We collected 1D ^{13}C and ^{15}N cross-polarization spectra that were recorded at $\omega_{0H}/2\pi$=800 MHz. We note that the ^{13}C cross polarized spectrum (**Figure 3A**) of Aβ$_{1-42}$ is slightly more well resolved than Aβ$_{M01-42}$, possibly due to a more compact core structure, but is otherwise comparable with respect to

chemical shifts. Similarly, the amide region of the ^{15}N cross polarization spectrum of $A\beta_{1-42}$ (**Figure 3C**) is similar to that of $A\beta_{M01-42}$. However, there are some differences in the side chains. The lysine signal for $A\beta_{1-42}$ fibrils consists of two lines with one more intense than the other and the arginine resonances are more intense than they are in $A\beta_{M01-42}$ fibrils. In the case of the lysine signals we assigned the more intense component to K28 and the latter to K16 that is difficult to observe in $A\beta_{M01-42}$ in 2D and 3D spectra.[17] Similar statements are applicable to the R5 resonances in $A\beta_{M01-42}$ where we observed that the

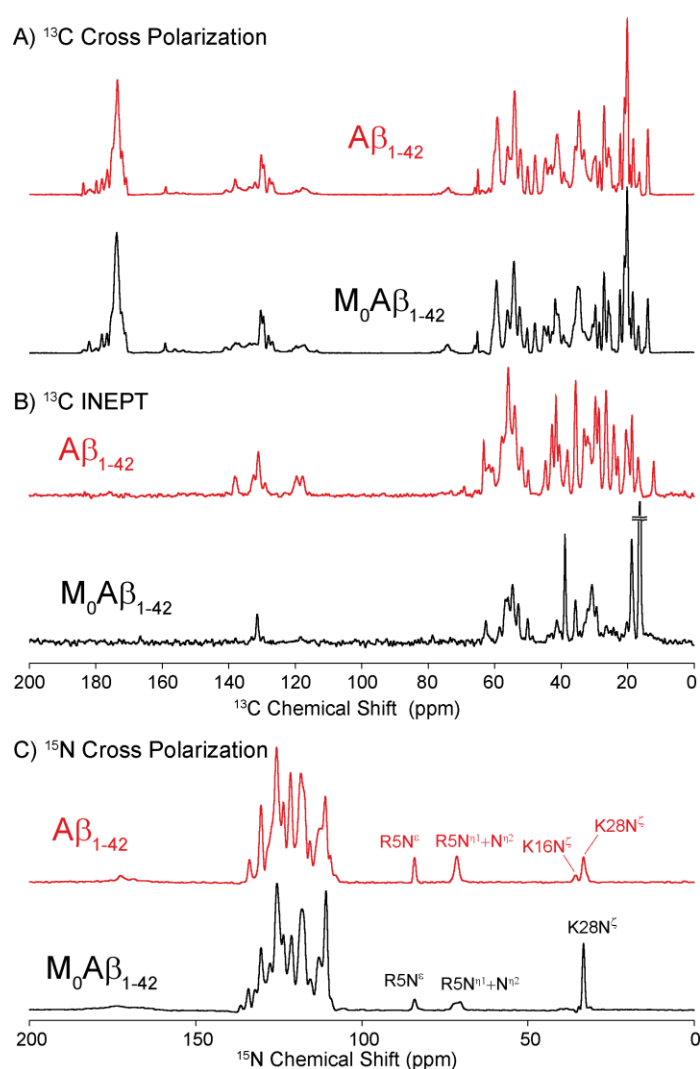**Figure 3:** 1D MAS NMR spectra of $A\beta_{1-42}$ (red) and $A\beta_{M01-42}$ (black) recorded at $\omega_{0H}/2\pi = 800$ MHz at 277 K and $\omega_r/2\pi = 20$ kHz with 83 kHz ^1H decoupling during acquisition. (a) ^{13}C cross polarization 1D spectrum recorded with 512 transients. (b) ^{13}C-INEPT spectrum recorded with 1024 transients. (c) ^{15}N cross polarization 1D spectrum recorded with 512 transients.

N^ε and $N^{\eta 1}$ and $N^{\eta 2}$ are attenuated indicating that R5 is more dynamic on a ns-µs time-scale in $A\beta_{M01-42}$. Finally, the ^{15}N-His resonances at ~180 ppm are broadened probably due to exchange and dynamics on a ns-µs time-scale. We note that the histidine ^{15}N tensors are large[71] and therefore sensitive to both to the dynamics and protonation state of the histidine side-chain. To visualize any dynamic regions of these amyloid fibrils, we recorded a 1D INEPT spectrum (**Figure 3B**), which appears to have more intense signals than observed previously, due to the absence of the N-terminal methionine, which had a very efficient transfer based on J-couplings. The increase in spectral intensity in the ^{13}C aromatic region is probably due to F4 (*vide infra*).

The fibrils of $A\beta_{M01-42}$ are structurally heterogeneous - the N-terminal 15 residues (M0-H14) are flexible and show only weak resonances in dipolar recoupling experiments, while the C-terminal core (Q15-A42) forms a rigid uniform structure. Initial studies suggested that fibrils of $A\beta_{1-42}$ may have both a slightly expanded rigid region, particularly with respect to the protein side chains. Moreover, removal of the first methionine residue appears to result in greater mobility in the N-terminal tail as evidenced by the increase in the chemical shifts and intensity of the J-coupled spectra. Thus, we will use homo and heteronuclear correlation spectroscopy to determine the differences in both the amyloid core and mobile N-terminal tail between $A\beta_{1-42}$ and $A\beta_{M01-42}$.

The rigid core structures of Aβ₁₋₄₂ and AβM01-42 fibrils are identical. To further explore the similarities and differences between the fibril core of $A\beta_{1-42}$ and $A\beta_{M01-42}$ we recorded ^{13}C-^{13}C RFDR[72] and ^{13}C-^{15}N ZF-TEDOR[73] (**Figure 4**). We collected these spectra using short dipolar mixing times and these spectra report on one and two bond correlations. To probe for longer-range correlations we also collected a ^{13}C-^{13}C DARR[74] spectrum with a longer mixing time (**Figure 5**). We have recently published a list of assignments for $A\beta_{M01-42}$[17] and used spectra recorded on that sample as a baseline to compare with the

Aβ₁₋₄₂ fibrils discussed herein. In the Aβ₁₋₄₂ spectra we observed a single set of chemical shifts indicating that only one fibril form is present. Polymorphism were not observed for the fibril core, consistent with our previous observations.[17] Furthermore the chemical shifts were virtually identical in Aβ₁₋₄₂ and AβM01-42 indicating that the fibril core is unchanged by the presence of the N-terminal methionine. However, we observed subtle differences between the two fibrils; we found that 1) some signals were much stronger in Aβ₁₋₄₂ than in AβM01-42, 2) minor chemical shift perturbations and 3) a

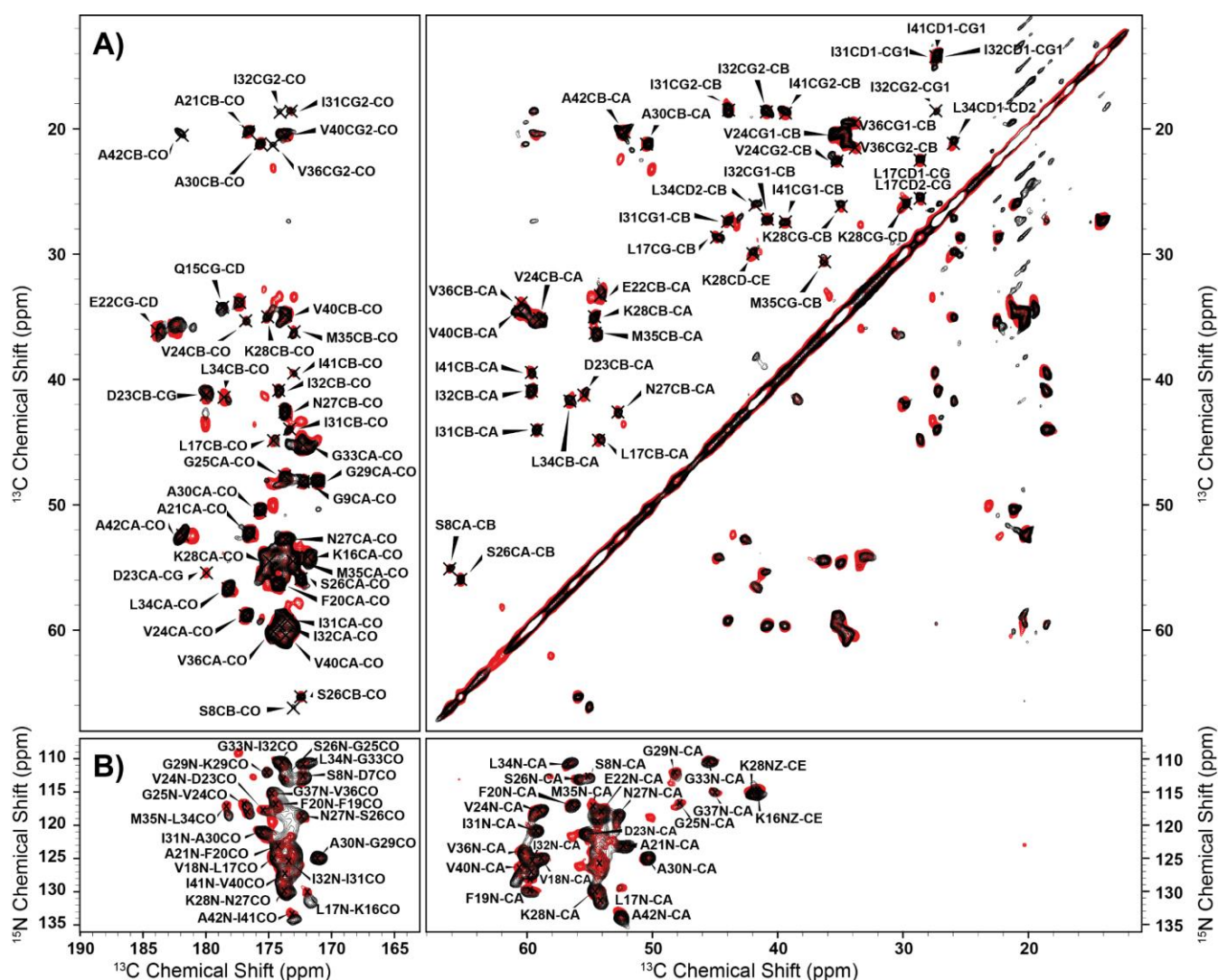**Figure 4:** (A) 1.6 ms mixing RFDR spectra of Aβ₁₋₄₂ (red) and AβM01-42 (black) recorded at 800 MHz, $\omega_r/2\pi$=20 kHz, VT gas regulated to 277 K with 83 kHz CW ¹H decoupling during evolution, and 83 kHz TPPM ¹H decoupling during acquisition. (B) 1.6 ms mixing ZF-TEDOR spectra of Aβ₁₋₄₂ (red) and AβM01-42 (black) recorded at 800 MHz, $\omega_r/2\pi$=20 kHz, VT gas regulated to 277K with 83 kHz TPPM during acquisition.

small number of additional peaks in the spectra of Aβ$_{1-42}$ fibrils. The resonance signals in Aβ$_{1-42}$ that most prominently exhibited increased intensity were A21, E22 and D23 (**Figure 4**). These peaks were considerably weaker in spectra of Aβ$_{M01-42}$. Interestingly, these residues reside in the 'toxic corner' of the recently published structure of Aβ$_{M01-42}$ that showed increased flexibility for these residues compared to the rest of the fibril core. However, it is not clear if these intensity variations are due to the presence or absence of the N-terminal methionine or if these occur for some other reason such as minor variations in pH or ionic strength during fibril growth.

Furthermore, most resonances of the fibril core show no or only minor chemical shift perturbations (CSP) between the Aβ$_{M01-42}$ and Aβ$_{1-42}$ and the results of the chemical shift analysis are
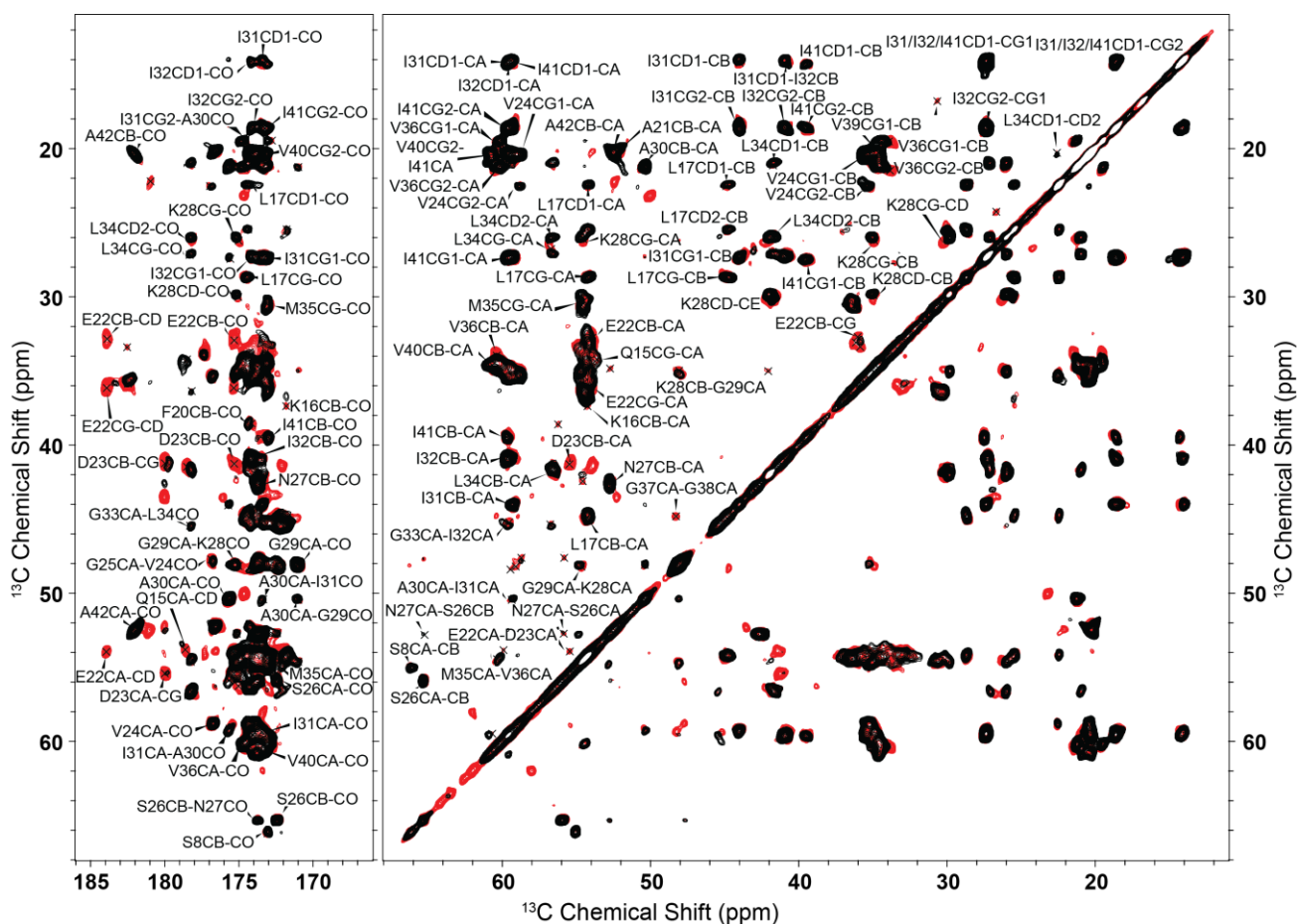

Figure 5. 2D ^{13}C-^{13}C-T DARR of Aβ$_{1-42}$ (red) and Aβ$_{M01-42}$ (blue) recorded at T= 277K, ω$_{0H}$/2π= 800 MHz, ω$_r$/2π= 20 kHz, and τ$_{mix}$(DARR) = 100 ms. A 83 kHz ^{1}H decoupling field was applied during acquisition.

summarized pictorially in **Figure 6**. The most prominent difference is at K16 and amounts to ~0.37 ppm

and V36 and which is 0.23 ppm. K16 is the residue that is directly adjacent to the beginning of the

disordered region in $A\beta_{M01\text{-}42}$ fibrils (**Figure 6B, red**). Because the other differences were smaller than

0.15 ppm, which is less than the error in our experiments, we conclude that M_0 does not have a

significant effect on the structure of the $A\beta_{1\text{-}42}$ core.

Interestingly, there are several peaks present in the ^{13}C-^{13}C RFDR and ^{13}C-^{15}N ZF-TEDOR

(**Figure 4**), as well as ^{13}C-^{13}C DARR spectra (**Figure 5**) that do not originate from chemical shift

perturbations or increased rigidity. Most likely, these resonances belong to residues of the N-terminal

tail in a second, more rigid conformation as evidenced by a second resonance in the ^{3}C-^{13}C RFDR and

^{13}C-^{15}N ZF-TEDOR, as well as ^{13}C-^{13}C DARR spectra at 56-62 ppm most likely belonging to S8. This

observation is in agreement with studies on $A\beta_{1\text{-}42}$ by Meier and co-workers that show polymorphism in
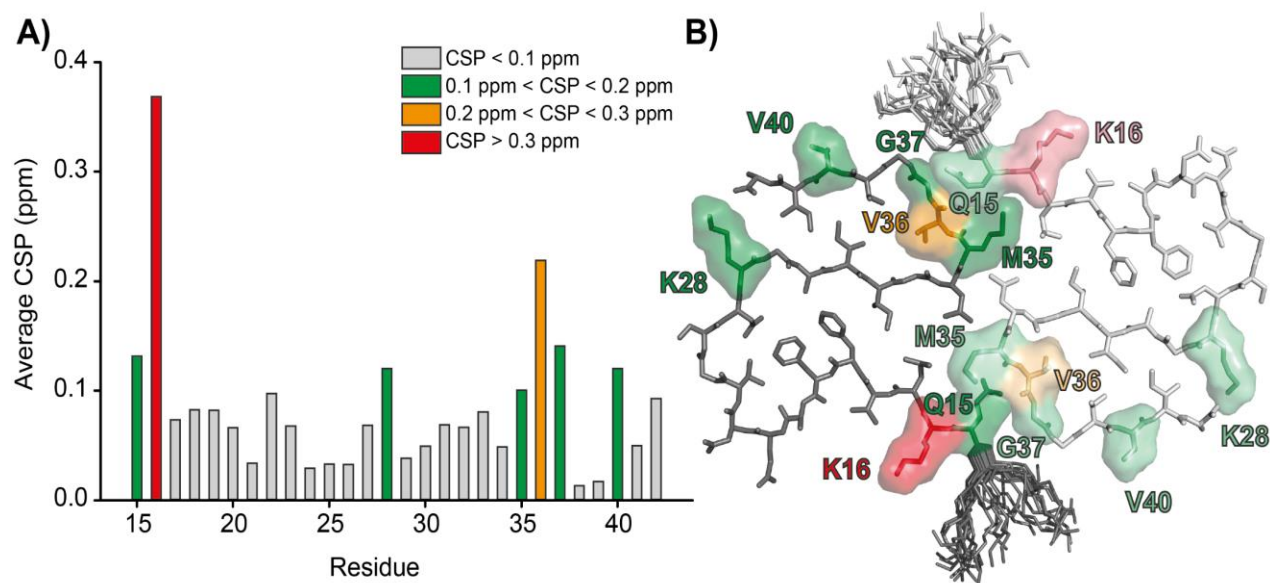
the absence of zinc during fibrillization.[19]

Figure 6: (A) ^{13}C chemical shift perturbations (CSP) between $A\beta_{M01\text{-}42}$ and $A\beta_{1\text{-}42}$ plotted as a function of residue position. The only residues where the shifts differ significantly are K16 and V36. (B) Structure of $A\beta_{M01\text{-}42}$ illustrating the positions of K16 and V36 and other residues with 0.1<CSP<0.2.

The N-terminal tail of Aβ₁-₄₂. Having determined that the N-terminal methionine does not significantly

impact the fibril core, we next sought to determine what difference, if any, would be observed on the N-

terminus, which is known to be flexible. We recorded a 2D INEPT-^{13}C-^{13}C TOBSY[75] (**Figure 5**)

spectrum. Leaving aside the obvious difference that results from the additional methionine in Aβ$_{M01-42}$,

the most apparent differences were for the aromatic resonances of F4, which were more intense in

spectra of Aβ$_{1-42}$ fibers than in Aβ$_{M01-42}$ fibrils. (**Figure 7, see also Figure 3**). As indicated in the INEPT

spectra (**Figure 3**), the INEPT-TOBSY spectra demonstrate that Aβ$_{1-42}$ has several flexible residues, and

that some, but not all of these residues are distinct from those in Aβ$_{M01-42}$. Overall this suggests that M0

may change the mobility of the flexible N-terminus by predisposing this region to sample a variety of

transient interactions with the amyloid core that are non-specifically driven by the hydrophobicity of the

methionine side chain. When the methionine is removed, the energetically preferred interaction point

between the flexible tail and the core uses F4 as a tether point, leading to a small number of additional

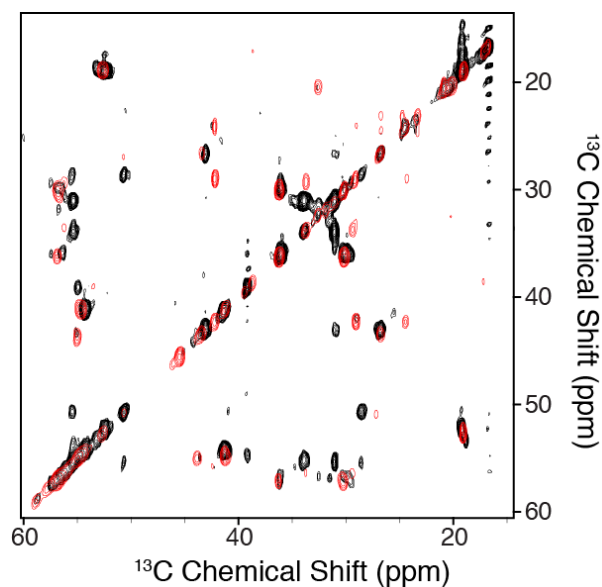**Figure 7.** 2D ^{13}C-^{13}C-TOBSY of Aβ$_{1-42}$ (red) and Aβ$_{M01-42}$ (blue)
recorded at T= 277K, $\omega_{0H}/2\pi$= 800 MHz, $\omega_r/2\pi$= 20 kHz, and
τ_{mix}(TOBSY) = 9.6 ms. A 83 kHz ^{1}H decoupling field was applied
during acquisition.

peaks in the dipolar–selective spectra.

Conclusions

We report a new preparation method to produce and purify $A\beta_{1-42}$ in sufficient yield to produce samples for MAS NMR spectroscopy. Monomers isolated by size exclusion chromatography can be incubated to yield fibrils of a monomorphic fibril core that exhibits excellent resolution and permitted us to determine a structure whose core is identical to that of $A\beta_{M01-42}$. In particular, by comparing the MAS NMR spectra of $A\beta_{1-42}$ with and without an N-terminal methionine, we determined that this residue has little impact on the structure of the fibril's core, as the chemical shifts are nearly identical between the two different species. Yet, despite this striking structural conservation, we found that the deletion of the N-terminal methionine residue changes these fibers in subtle ways. $A\beta_{1-42}$ fibers are more rigid than $A\beta_{M01-42}$ fibers, which is seen as a small increase in the number of interactions (a handful of new peaks become visible) and a change in the dynamics of some regions of the core (increased peak intensities, particularly in the "toxic corner" of the fibril). Because $A\beta_{1-42}$ and $A\beta_{M01-42}$ follow the same aggregation mechanism with highly similar rate constants and because these dynamic differences are minor, structural studies that use an $A\beta_{M01-42}$ should be generalizable to $A\beta_{1-42}$. However, investigations of the role of the disordered regions and their possible interactions should consider M0 as a variable.

REFERENCES

[1] Chiti, F., and Dobson, C. (2006) Protein misfolding, functional amyloid, and human disease., *Annu Rev Biochem 75*, 333-366.

[2] Dobson, C. M. (2006) Protein aggregation and its consequences for human disease, *Protein Peptide Lett 13*, 219-227.

[3] Comellas, G., Lemkau, L. R., Nieuwkoop, A. J., Kloepper, K. D., Ladror, D. T., Ebisu, R., Woods, W. S., Lipton, A. S., George, J. M., and Rienstra, C. M. (2011) Structured Regions of alpha-Synuclein Fibrils Include the Early-Onset Parkinson's Disease Mutation Sites, *J Mol Biol 411*, 881-895.

[4] Heise, H., Hoyer, W., Becker, S., Andronesi, O. C., Riedel, D., and Baldus, M. (2005) Molecular-level secondary structure, polymorphism, and dynamics of full-length alpha-synuclein fibrils studied by solid-state NMR, *Proc. Natl. Acad. Sci. U.S.A. 102*, 15871-15876.

[5] Olanow, C. W., and Brundin, P. (2013) Parkinson's Disease and Alpha Synuclein: Is Parkinson's Disease a Prion-Like Disorder?, *Movement Disord 28*, 31-40.

[6] Vilar, M., Chou, H. T., Luhrs, T., Maji, S. K., Riek-Loher, D., Verel, R., Manning, G., Stahlberg, H., and Riek, R. (2008) The fold of alpha-synuclein fibrils, *Proc. Natl. Acad. Sci. U.S.A. 105*, 8637-8642.

[7] Marzban, L., Park, K., and Verchere, C. B. (2003) Islet amyloid polypeptide and type 2 diabetes, *Exp Gerontol 38*, 347-351.

[8] Westermark, P., Andersson, A., and Westermark, G. T. (2011) Islet amyloid polypeptide, islet amyloid, and diabetes mellitus, *Physiol Rev 91*, 795-826.

[9] Debelouchina, G. T., Platt, G. W., Bayro, M. J., Radford, S. E., and Griffin, R. G. (2010) Intermolecular Alignment in beta(2)-Microglobulin Amyloid Fibrils, *J Am Chem Soc 132*, 17077-17079.

[10] Debelouchina, G. T., Platt, G. W., Bayro, M. J., Radford, S. E., and Griffin, R. G. (2010) Magic Angle Spinning NMR Analysis of beta(2)-Microglobulin Amyloid Fibrils in Two Distinct Morphologies, *J Am Chem Soc 132*, 10414-10423.

[11] De Strooper, B., Saftig, P., Craessaerts, K., Vanderstichele, H., Guhde, G., Annaert, W., Von Figura, K., and Van Leuven, F. (1998) Deficiency of presenilin-1 inhibits the normal cleavage of amyloid precursor protein, *Nature 391*, 387-390.

[12] Vassar, R., Bennett, B. D., Babu-Khan, S., Kahn, S., Mendiaz, E. A., Denis, P., Teplow, D. B., Ross, S., Amarante, P., Loeloff, R., Luo, Y., Fisher, S., Fuller, L., Edenson, S., Lile, J., Jarosinski, M. A., Biere, A. L., Curran, E., Burgess, T., Louis, J. C., Collins, F., Treanor, J., Rogers, G., and Citron, M. (1999) beta-secretase cleavage of Alzheimer's amyloid precursor protein by the transmembrane aspartic protease BACE, *Science 286*, 735-741.

[13] Jarrett, J. T., Berger, E. P., and Lansbury, P. T. (1993) The Carboxy Terminus of the Beta-Amyloid Protein Is Critical for the Seeding of Amyloid Formation - Implications for the Pathogenesis of Alzheimers-Disease, *Biochemistry-Us 32*, 4693-4697.

[14] Jarrett, J. T., Berger, E. P., and Lansbury, P. T., Jr. (1993) The C-terminus of the beta protein is critical in amyloidogenesis, *Ann N Y Acad Sci 695*, 144-148.

[15] Meisl, G., Yang, X. T., Hellstrand, E., Frohm, B., Kirkegaard, J. B., Cohen, S. I. A., Dobson, C. M., Linse, S., and Knowles, T. P. J. (2014) Differences in nucleation behavior underlie the contrasting aggregation kinetics of the A beta 40 and A beta 42 peptides, *Proc. Natl. Acad. Sci. U.S.A. 111*, 9384-9389.

[16] Finder, V. H., Vodopivec, I., Nitsch, R. M., and Glockshuber, R. (2010) The Recombinant Amyloid-beta Peptide A beta 1-42 Aggregates Faster and Is More Neurotoxic than Synthetic A beta 1-42, *J Mol Biol 396*, 9-18.

[17] Colvin, M. T., Silvers, R., Frohm, B., Su, Y., Linse, S., and Griffin, R. G. (2015) High Resolution Structural Characterization of Aβ42 Amyloid Fibrils by MAS NMR, *J. Am. Chem. Soc. 137*, 7509–7518

[18] Colvin, M. T., Silvers, R., Ni, Q. Z., Can, T. V., Sergeyev, I., Rosay, M., Donovan, K. J., Michael, B., Wall, J., Linse, S., and Griffin, R. G. (2016) Atomic Resolution Structure of Monomorphic Aβ42 Amyloid Fibrils, *J Am Chem Soc 138*, 9663–9674.

[19] Wälti, M. A., Ravotti, F., Arai, H., Glabe, C. G., Wall, J. S., Böckmann, A., Güntert, P., Meier, B. H., and Riek, R. (2016) Atomic-resolution structure of a disease-relevant Aβ(1–42) amyloid fibril, *Proc. Natl. Acad. Sci. U.S.A. 113*, E4976–E4984.

[20] Cukalevski, R., Yang, X., Meisl, G., Weininger, U., Bernfur, K., Birgitta, Frohm, Knowles, T. P. J., and Linse, S. (2015) The Aβ40 and Aβ42 peptides self-assemble into separate homomolecular fibrils in binary mixtures but cross-react during primary nucleation, *Chemical Science 6*, 4215-4233.

[21] Aguzzi, A., and O'Connor, T. (2010) Protein aggregation diseases: pathogenicity and therapeutic perspectives, *Nat. Rev. Drug Discov. 9*, 237–248.

[22] Haass, C., and Selkoe, D. J. (2007) Soluble protein oligomers in neurodegeneration: lessons from the Alzheimer's amyloid β-peptide, *Nat. Rev. Mol. Cell Biol. 8*, 101-112.

[23] Koo, E. H., Lansbury, P. T. J., and Kelly, J. W. (1999) Amyloid diseases: abnormal protein aggregation in neurodegeneration, *Proc. Natl. Acad. Sci. U.S.A. 96*, 9989–9990.

[24] Tycko, R. (2011) Solid-State NMR Studies of Amyloid Fibril Structure, *Annu Rev Phys Chem 62*, 279-299.

[25] Debelouchina, G. T., Bayro, M. J., Fitzpatrick, A. W., Ladizhansky, V., Colvin, M. T., Caporini, M. A., Jaroniec, C. P., Bajaj, V. S., Rosay, M., MacPhee, C. E., Vendruscolo, M., Maas, W. E., Dobson, C. M., and Griffin, R. G. (2013) Higher Order Amyloid Fibril Structure by MAS NMR and DNP Spectroscopy, *J Am Chem Soc 135*, 19237-19247.

[26] Tanzi, R. E., and Bertram, L. (2005) Twenty years of the Alzheimer's disease amyloid hypothesis: a genetic perspective, *Cell 120*, 545–555.

[27] Lansbury, P. T., Costa, P. R., Griffiths, J. M., Simon, E. J., Auger, M., Halverson, K. J., Kocisko, D. A., Hendsch, Z. S., Ashburn, T. T., Spencer, R. G. S., Tidor, B., and Griffin, R. G. (1995) Structural model for the [beta]-amyloid fibril based on interstrand alignment of an antiparallel-sheet comprising a C-terminal peptide, *Nature structural & molecular biology 2*, 990-998.

[28] Antzutkin, O. N., Balbach, J. J., Leapman, R. D., Rizzo, N. W., Reed, J., and Tycko, R. (2000) Multiple quantum solid-state NMR indicates a parallel, not antiparallel, organization of beta-sheets in Alzheimer's beta-amyloid fibrils, *Proc. Natl. Acad. Sci. U.S.A. 97*, 13045-13050.

[29] Petkova, A. T., Ishii, Y., Balbach, J. J., Antzutkin, O. N., Leapman, R. D., Delaglio, F., and Tycko, R. (2002) A structural model for Alzheimer's beta-amyloid fibrils based on experimental constraints from solid state NMR, *Proc. Natl. Acad. Sci. U.S.A. 99*, 16742-16747.

[30] Bayro, M. J., Maly, T., Birkett, N., MacPhee, C., Dobson, C. M., and Griffin, R. G. (2010) High-resolution MAS NMR analysis of PI3-SH3 amyloid fibrils: Backbone conformation and implications for protofilament assembly and structure, *Biochemistry-Us 49*, 7474-7488.

[31] Bayro, M. J., Debelouchina, G. T., Eddy, M. T., Birkett, N. R., MacPhee, C. E., Rosay, M., Maas, W. E., Dobson, C. M., and Griffin, R. G. (2011) Intermolecular structure determination of amyloid fibrils with magic-angle spinning, dynamic nuclear polarization NMR, *J. Am. Chem. Soc. 133*, 13967–13974.

[32] Debelouchina, G. T., Platt, G. W., Bayro, M. J., Radford, S. E., and Griffin, R. G. (2010) Intermolecular Alignment in β2-Microglobulin Amyloid Fibrils, *J Am Chem Soc 132*, 17077–17079.

[33] Sarell, C. J., Woods, L. A., Su, Y., Debelouchina, G. T., Ashcroft, A. E., Griffin, R. G., Stockley, P. G., and Radford, S. E. (2013) Expanding the repertoire of amyloid polymorphs by co-polymerization of related protein precursors, *J. Biol. Chem. 288*, 7327–7337.

[34] Su, Y. C., Sarell, C. J., Eddy, M. T., Debelouchina, G. T., Andreas, L. B., Pashley, C. L., Radford, S. E., and Griffin, R. G. (2014) Secondary Structure in the Core of Amyloid Fibrils Formed from Human beta(2)m and its Truncated Variant Delta N6, *J Am Chem Soc 136*, 6313-6325.

[35] Comellas, G., Lemkau, L. R., Zhou, D. H. H., George, J. M., and Rienstra, C. M. (2012) Structural Intermediates during alpha-Synuclein Fibrillogenesis on Phospholipid Vesicles, *J Am Chem Soc 134*, 5090-5099.

[36] Gath, J., Bousset, L., Habenstein, B., Melki, R., Meier, B. H., and Bockmann, A. (2014) Yet another polymorph of alpha-synuclein: solid-state sequential assignments, *Biomolecular NMR Assignments 8*, 395-404.

[37] Gath, J., Habenstein, B., Bousset, L., Melki, R., Meier, B. H., and Bockmann, A. (2012) Solid-state NMR sequential assignments of alpha-synuclein, *Biomolecular NMR Assignments 6*, 51-55.

[38] Kloepper, K. D., Hartman, K. L., Ladror, D. T., and Rienstra, C. M. (2007) Solid-state NMR spectroscopy reveals that water is nonessential to the core structure of alpha-synuclein fibrils, *Journal of Physical Chemistry B 111*, 13353-13356.

[39] Kloepper, K. D., Woods, W. S., Winter, K. A., George, J. M., and Rienstra, C. M. (2006) Preparation of alpha-synuclein fibrils for solid-state NMR: Expression, purification, and incubation of wild-type and mutant forms, *Protein Expres Purif 48*, 112-117.

[40] Kloepper, K. D., Zhou, D. H., Li, Y., Winter, K. A., George, J. M., and Rienstra, C. M. (2007) Temperature-dependent sensitivity enhancement of solid-state NMR spectra of alpha-synuclein fibrils, *Journal of Biomolecular NMR 39*, 197-211.

[41] Lemkau, L. R., Comellas, G., Kloepper, K. D., Woods, W. S., George, J. M., and Rienstra, C. M. (2012) Mutant Protein A30P alpha-Synuclein Adopts Wild-type Fibril Structure, Despite Slower Fibrillation Kinetics, *J. Biol. Chem. 287*, 11526-11532.

[42] Lemkau, L. R., Comellas, G., Lee, S. W., Rikardsen, L. K., Woods, W. S., George, J. M., and Rienstra, C. M. (2013) Site-Specific Perturbations of Alpha-Synuclein Fibril Structure by the Parkinson's Disease Associated Mutations A53T and E46K, *Plos One 8*.

22

[43] Woods, W. S., Boettcher, J. M., Zhou, D. H., Kloepper, K. D., Hartman, K. L., Ladror, D. T., Qi, Z., Rienstra, C. M., and George, J. M. (2007) Conformation-specific binding of alpha-synuclein to novel protein partners detected by phage display and NMR spectroscopy, *J. Biol. Chem. 282*, 34555-34567.

[44] Bousset, L., Pieri, L., Ruiz-Arlandis, G., Gath, J., Jensen, P. H., Habenstein, B., Madiona, K., Olieric, V., Bockmann, A., Meier, B. H., and Melki, R. (2013) Structural and functional characterization of two alpha-synuclein strains, *Nat Commun 4*.

[45] Lv, G. H., Kumar, A., Giller, K., Orcellet, M. L., Riedel, D., Fernandez, C. O., Becker, S., and Lange, A. (2012) Structural Comparison of Mouse and Human alpha-Synuclein Amyloid Fibrils by Solid-State NMR, *J Mol Biol 420*, 99-111.

[46] Mollenhauer, B., Trautmann, E., Otte, B., Ng, J., Spreer, A., Lange, P., Sixel-Doring, F., Hakimi, M., VonSattel, J. P., Nussbaum, R., Trenkwalder, C., and Schlossmacher, M. G. (2012) alpha-Synuclein in human cerebrospinal fluid is principally derived from neurons of the central nervous system, *J Neural Transm 119*, 739-746.

[47] Kim, H. Y., Cho, M. K., Kumar, A., Maier, E., Siebenhaar, C., Becker, S., Fernandez, C. O., Lashuel, H. A., Benz, R., Lange, A., and Zweckstetter, M. (2009) Structural Properties of Pore-Forming Oligomers of alpha-Synuclein, *J Am Chem Soc 131*, 17482-17489.

[48] Ahmed, M., Davis, J., Aucoin, D., Sato, T., Ahuja, S., Aimoto, S., Elliott, J. I., Van Nostrand, W. E., and Smith, S. O. (2010) Structural conversion of neurotoxic amyloid-beta(1-42) oligomers to fibrils, *Nature structural & molecular biology 17*, 561-U556.

[49] Fandrich, M., Schmidt, M., and Grigorieff, N. (2011) Recent progress in understanding Alzheimer's beta-amyloid structures, *Trends in Biochemical Sciences 36*, 338-345.

[50] Miller, Y., Ma, B. Y., Tsai, C. J., and Nussinov, R. (2010) Hollow core of Alzheimer's A beta(42) amyloid observed by cryoEM is relevant at physiological pH, *Proc. Natl. Acad. Sci. U.S.A. 107*, 14128-14133.

[51] Zhang, R., Hu, X. Y., Khant, H., Ludtke, S. J., Chiu, W., Schmid, M. F., Frieden, C., and Lee, J. M. (2009) Interprotofilament interactions between Alzheimer's A beta(1-42) peptides in amyloid fibrils revealed by cryoEM, *Proc. Natl. Acad. Sci. U.S.A. 106*, 4653-4658.

[52] Tay, W. M., Huang, D. T., Rosenberry, T. L., and Paravastu, A. K. (2013) The Alzheimer's Amyloid-beta(1-42) Peptide Forms Off-Pathway Oligomers and Fibrils That Are Distinguished Structurally by Intermolecular Organization, *J Mol Biol 425*, 2494-2508.

[53] Eddy, M. T., Belenky, M., Sivertsen, A. C., Griffin, R. G., and Herzfeld, J. (2013) Selectively dispersed isotope labeling for protein structure determination by magic angle spinning NMR, *Journal of Biomolecular NMR 57*, 129-139.

[54] Walsh, D. M., Thulin, E., Minogue, A. M., Gustavsson, N., Pang, E., Teplow, D. B., and Linse, S. (2009) A facile method for expression and purification of the Alzheimer's disease-associated amyloid beta-peptide, *Febs J 276*, 1266-1281.

[55] Portelius, E., G, B., AJ, T., H, Z., A, W.-B., and K, B. (2009) Identification of novel APP/Abeta isoforms in human cerebrospinal fluid, *Neurodeg. Discussions 6*, 87-94.

[56] Kaneko, N., Yamamoto, R., Sato, T.-A., and Tanaka, K. (2014) Identification and quantification of amyloid beta-related peptides in human plasma using matrix-assisted laser desorption/ionization time-of-flight mass spectrometry, *Proc. Japan. Acad. Ser. B 90*, 104-117.

[57] Szczepankiewicz, O., Linse, B., Meisl, G., Thulin, E., Frohm, B., Frigerio, C. S., Colvin, M. T., Jacavone, A. C., Griffin, R. G., Knowles, T., Walsh, D. M., and Linse, S. (2015) N-Terminal Extensions Retard A beta 42 Fibril Formation but Allow Cross-Seeding and Coaggregation with A beta 42, *J Am Chem Soc 137*, 14673-14685.

[58] Cohen, S. I., Linse, S., Luheshi, L. M., Hellstrand, E., White, D. A., Rajah, L., Otzen, D. E., Vendruscolo, M., Dobson, C. M., and Knowles, T. P. (2013) Proliferation of amyloid-beta42 aggregates occurs through a secondary nucleation mechanism, *Proc. Natl. Acad. Sci. U.S.A. 110*, 9758-9763.

[59] Zhang, L., Yu, H., Song, C., Lin, X., Chen, B., Tan, C., Cao, G., and Wang, Z. (2009) Expression, purification, and characterization of recombinant human b-amyloid42 peptide in Escherichia coli, *Protein Expres Purif 64*, 55-62.

[60] Long, F., Cho, W., and Ishii, Y. (2011) Expression and purification of N-15- and C-13-isotope labeled 40-residue human Alzheimer's beta-amyloid peptide for NMR-based structural analysis, *Protein Expres Purif 79*, 16-24.

[61] Lee, E. K., Hwang, J. H., Shin, D. Y., Kim, D. I., and Yoo, Y. J. (2005) Production of recombinant amyloid-beta peptide 42 as an ubiquitin extension, *Protein Expres Purif 40*, 183-189.

[62] Garai, K., Crick, S. L., Mustafi, S. M., and Frieden, C. (2009) Expression and purification of amyloid-beta peptides from Escherichia coli, *Protein Expres Purif 66*, 107-112.

[63] Nagata-Uchiyama, M., Yaguchi, M., Hirano, Y., and Ueda, T. (2007) Expression and purification of uniformly N-15-Labeled amyloid p peptide 1-40 in Escherichia coli, *Protein Peptide Lett 14*, 788-792.

[64] Ovchinnikova, O. Y., Finder, V. H., Vodopivec, I., Nitsch, R. M., and Glockshuber, R. (2011) The Osaka FAD Mutation E22 Delta Leads to the Formation of a Previously Unknown Type of Amyloid beta Fibrils and Modulates A beta Neurotoxicity, *J Mol Biol 408*, 780-791.

[65] Satakarni, M., and Curtis, R. (2011) Production of recombinant peptides as fusions with SUMO, *Protein Expres Purif 78*, 113-119.

[66] Weber, D. K., Sani, M. A., and Gehman, J. D. (2014) A routine method for cloning, expressing and purifying Aβ(1–42) for structural NMR studies, *Amino Acids 46*, 2415–2426.

[67] Andreasson, C., Fiaux, J., Rampelt, H., Mayer, M. P., and Bukau, B. (2008) Hsp110 is a nucleotide-activated exchange factor for Hsp70, *J. Biol. Chem. 283*, 8877-8884.

[68] Meisl, G., Kirkegaard, J. B., Arosio, P., Michaels, T. C. T., Vendruscolo, M., Dobson, C. M., Linse, S., and Knowles, T. P. J. (2016) Molecular mechanisms of protein aggregation from global fitting of kinetic models, *Nature Protocols 11*, 252-272.

[69] Goddard, T. D., and Kneller, D. G. (2008) SPARKY Version 3.115, Univ. California, San Francisco.

[70] Cohen, S. I. A., Vendruscolo, M., Dobson, C. M., and Knowles, T. P. J. (2012) From Macroscopic Measurements to Microscopic Mechanisms of Protein Aggregation, *J Mol Biol 421*, 160-171.

[71] Munowitz, M., Bachovchin, W. W., Herzfeld, J., Dobson, C. M., and Griffin, R. G. (1982) Acid-Base and Tautomeric Equilibria in the Solid-State - N-15 Nmr-Spectroscopy of Histidine and Imidazole, *J Am Chem Soc 104*, 1192-1196.

[72] Bennett, A. E., Ok, J. H., Griffin, R. G., and Vega, S. (1992) Chemical-Shift Correlation Spectroscopy in Rotating Solids - Radio Frequency-Driven Dipolar Recoupling and Longitudinal Exchange, *J Chem Phys 96*, 8624-8627.

[73] Jaroniec, C. P., Filip, C., and Griffin, R. G. (2002) 3D TEDOR NMR experiments for the simultaneous measurement of multiple carbon-nitrogen distances in uniformly C-13, N-15-labeled solids, *J Am Chem Soc 124*, 10728-10742.

[74] Takegoshi, K., Nakamura, S., and Terao, T. (2001) C-13-H-1 dipolar-assisted rotational resonance in magic-angle spinning NMR, *Chem Phys Lett 344*, 631-637.

[75] Andronesi, O. C., Becker, S., Seidel, K., Heise, H., Young, H. S., and Baldus, M. (2005) Determination of membrane protein structure and dynamics by magic-angle-spinning solid-state NMR spectroscopy, *J Am Chem Soc 127*, 12965-12974.